Performance Improvement of GaN-Based Vertical-Cavity Surface-Emitting Lasers by Using Tapered SiO_2-Buried Structure

Rongbin Xu, Yachao Wang, Mingchao Fang, Yang Mei, Leiying Ying, Daquan Yu, *Senior Member, IEEE*, and Baoping Zhang

***Abstract*—In GaN-based vertical-cavity surface-emitting lasers (VCSELs) with insulator-buried structure, the strong index guiding will introduce higher order modes. In this paper, we present a novel GaN-based VCSEL with a tapered SiO_2-buried structure by numerical simulations. Compared to conventional flat aperture VCSELs, tapered aperture VCSELs show the lower threshold current and higher slope efficiency, and can be attributed to the improvement of current distribution within the current injection aperture. Moreover, by adjusting the taper length, the current distribution in current injection aperture can be further changed, enabling single fundamental mode lasing. Additionally, the modulation bandwidth for tapered aperture VCSELs will also increase due to the reduction of parasitic capacitance. This research guides the development of high performance GaN VCSELs capable of achieving single transverse mode and high modulation rates for visible optical communication links and networks.**

***Index Terms*—GaN-based laser, numerical simulation, vertical-cavity surface-emitting laser (VCSEL), tapered aperture, modulation response.**

I. Introduction

In recent years, vertical-cavity surface-emitting lasers (VCSELs) have received great interest for applications in optical interconnects due to their potential for single-mode operation, desirable beam properties (circular and low divergence beam) and integration capabilities with other optoelectronic components [1], [2]. Among the candidates for making VCSELs, GaN-based compound semiconductors are expected to serve as active materials to achieve spectral illumination in ultraviolet to visible region. With the mature application of GaAs-based VCSELs in the field of optical communication [3], [4], GaN VCSELs begin to develop in the application of visible light communication, which requires GaN VCSELs with high performance, ensuring single transverse mode operation and high modulation rates [5], [6].

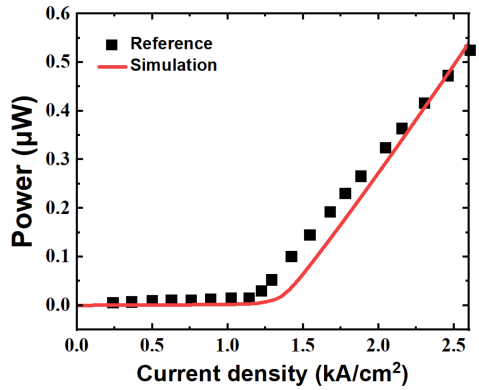

Fig. 1. P-I curves in experiments and simulations.

Effective lateral optical and electrical confinement is crucial for achieving high performance GaN VCSELs [7], [8]. In contrast to GaAs-based VCSELs, selective oxidation is difficult for GaN-based VCSELs due to the inherent properties of the material. Therefore, various approaches have been developed to achieve lateral confinement in GaN-based VCSELs, including ion implantation [9], [10], photoelectrochemically etched air-gap aperture [11], buried insulating layer [12], [13], [14], monolithic curved mirror [15], reactive ion etching (RIE) passivation [16], [17], et al. Among them, insulator-buried structure is rather simple and preferable. However, in GaN VCSELs with insulator-buried structure, the strong index guiding will introduce higher order modes. These modes are mainly distributed around the edge of the current injection aperture. As a result, the non-uniformity of current injection in the active region will introduce a certain degree of mode selectivity, usually favoring higher order modes [14], [18]. Up to now, to achieve fundamental mode lasing in VCSELs, suppressing higher order modes involves reducing the injection current aperture and increasing lateral losses [19]. However, the small aperture leads to a high series resistance and limits the output power because of excessive current induced self-heating. Increasing the loss requires additional processes, complicating device preparation. Therefore, it is challenging to realize single fundamental mode

Received 6 December 2024; accepted 22 December 2024. Date of publication 25 December 2024; date of current version 9 January 2025. This work was supported by the National Natural Science Foundation of China under Grant 62234011, Grant U21A20493, and Grant 62104204. *(Rongbin Xu and Yachao Wang contributed equally to this work.) (Corresponding author: Baoping Zhang.)*

Rongbin Xu, Yachao Wang, Mingchao Fang, Yang Mei, Leiying Ying, and Daquan Yu are with the School of Electronic Science and Engineering, Xiamen University, Xiamen 361005, China.

Baoping Zhang is with the School of Electronic Science and Engineering, Xiamen University, Xiamen 361005, China, and also with the Institute of Nanoscience and Applications (INA), Southern University of Science and Technology (SUSTech), Shenzhen 518055, China (e-mail: bzhang@xmu.edu.cn).

Digital Object Identifier 10.1109/JPHOT.2024.3522498

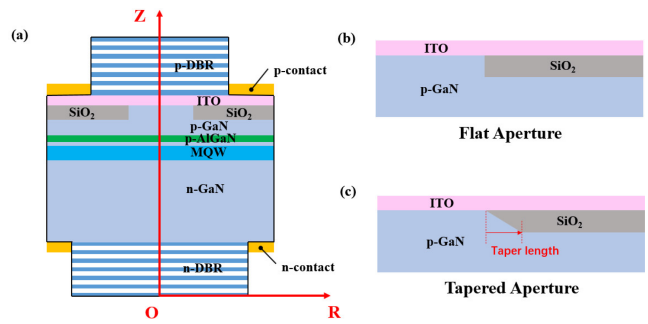

Fig. 2. (a) Schematic of GaN-based VCSEL with SiO_2-buried structure. (b) Schematic structure for flat and (c) tapered SiO_2-buried aperture. O, Z, R in (a) represent the original point, the vertical and lateral coordinate of simulation model, respectively. The red arrow in (c) indicates the taper length.

lasing, which seriously restricts the development of truly single-mode GaN VCSELs with insulator-buried structure.

In this work, a novel GaN-based VCSEL with tapered SiO_2-buried structure is proposed and theoretically investigated by numerical simulations. The simulation results showed that the threshold current and slope efficiency of VCSELs can be improved by introducing tapered aperture structure. By increasing taper length, fundamental mode lasing can be achieved. Moreover, since parasitic capacitance of the device is affected by SiO_2-buried layer, the modulation bandwidth of the device with different taper length were also investigated. This study provides reference significance for the realization of high performance GaN-based VCSEL.

II. Device Structure and Physical Model

To verify the accuracy of simulation model, we initially simulated a reference device as reported by Liu et al. [20]. The numerical simulations are performed by Crosslight PICS3D. The PICS3D is based on three-dimensional finite element analysis and the physical models such as current continuity equations, Poisson's equation, complex wave equations, and rate equations of VCSEL devices can be employed to solve the problems consistently in the cylindrical coordinates [21]. The transport model includes drift and diffusion of electrons and holes, Fermi statistics, as well as spontaneous and defect-related Shockley-Read-Hall (SRH) recombination of carriers. The spontaneous and piezoelectric polarization in GaN-based materials were considered in the simulator to calculate the built-in polarization field and the polarization level was set at 20%. The offset ratio of conduction/valence band in the MQWs was set to be 70:30. Since the cylindrical symmetry of the calculated VCSEL, the simulation model can be simplified into a two-dimensional axisymmetric structure. Fig. 1 presents the power-current (P-I) characterization for both the experimental VCSEL (black dots) and the simulated VCSEL (red line). The emission wavelength is 423 nm and the cavity length is 13λ. It can be observed that threshold current and slope efficiency of simulation fit well with measurement result.

In our proposed device, the GaN VCSEL has a dual dielectric DBR design. The current aperture is defined by SiO_2 insulating layer. The cavity of VCSEL consists of a 40 nm ITO current spreading layer, a 600 nm thick p-GaN layer with the doping concentration of 4×10^{17} cm^{-3}, a 20 nm thick p-$Al_{0.2}Ga_{0.8}N$ electron blocking layer (p-EBL) with doping concentration of 1×10^{18} cm^{-3}, 2 pairs of $In_{0.18}Ga_{0.82}N$ (2.5 nm)/GaN (6 nm) quantum wells (QWs) and a 2 μm n-GaN layer with the doping concentration of 2.5×10^{18} cm^{-3}. The schematic cross section of VCSEL with SiO_2-buried structure is shown in Fig. 2(a). Fig. 2(b) and (c) show the schematic diagrams of two kinds of confinement structures for VCSELs with flat and tapered aperture, respectively. To account for optical losses, the average optical background loss in the cavity was set to 1000 m^{-1}. In the optical mode model, both the longitudinal and transverse optical modes are solved by the effective index model (EIM).

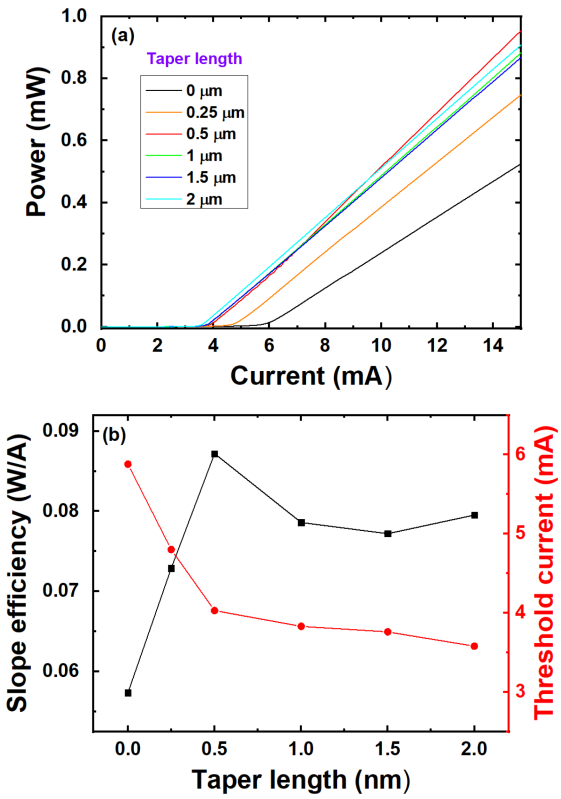

Fig. 3. (a) Simulated lasing power as a function of the injection current for VCSELs with different taper length. (b) Fitting slope efficiency and threshold current as a function of taper length. The flat aperture VCSEL has a taper length of 0 μm.

III. Simulation Results and Discussion

Fig. 3(a) shows the power-current (P-I) characterization of VCSELs with flat and tapered aperture. The conventional flat aperture VCSEL has a taper length of 0 μm. The studied VCSELs have the cavity length of ~16λ and the current injection aperture defined by SiO_2 has a diameter of 15 μm. Compared with flat aperture VCSEL, tapered aperture VCSELs shows the lower threshold current and higher slope efficiency. The VCSELs with different taper length were also simulated to further study the influence of the taper structure on the performance of GaN VCSELs. The fitting slope efficiency and threshold current are shown in Fig. 3(b). We can observe that the threshold current

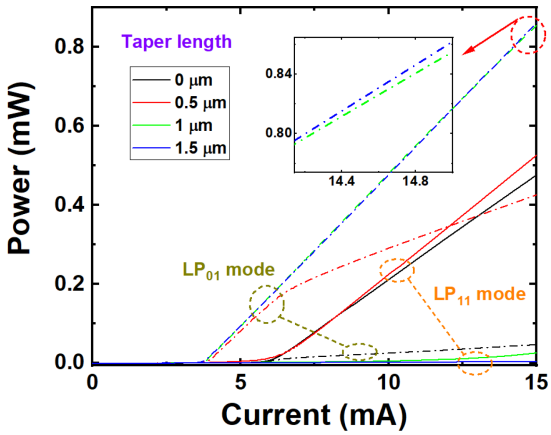

Fig. 4. P-I curves of LP_{01} and LP_{11} lasing modes for the VCSELs with different taper length. The dash dot and solid lines represent the LP_{01} and LP_{11} lasing modes, respectively. Inset shows the zoom-in lasing power of LP_{01} modes for VCSELs with 1 and 1.5 μm taper length.

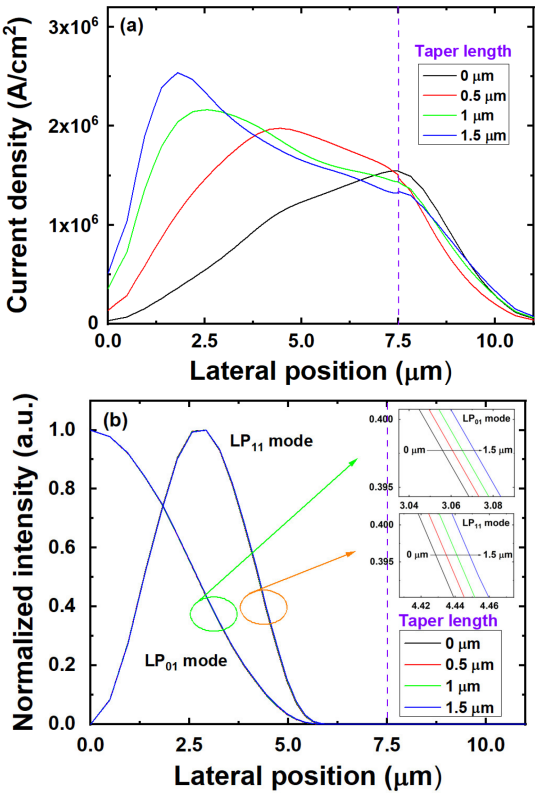

Fig. 5. (a) Current density and (b) optical mode distributions within the QWs along the lateral direction. The dash line presents the boundary inside and outside the current injection aperture.

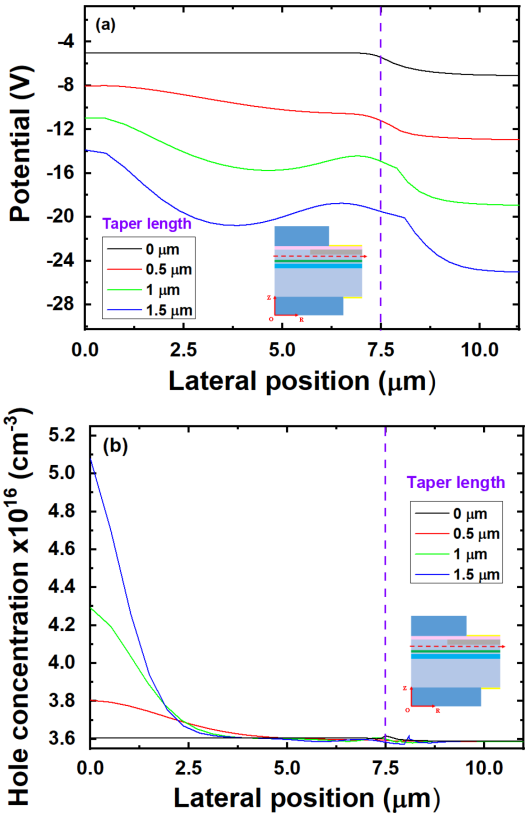

Fig. 6. (a) Lateral potential distribution and (b) hole concentrations in p-GaN below the SiO_2 layer at the current of 15 mA. The position is fixed to be 10 nm away from SiO_2 layer and marked by red dash line in the inset schematic VCSEL.

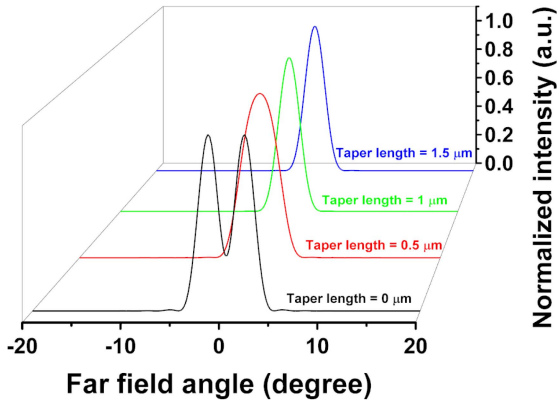

Fig. 7. Far-field distribution of VCSELs with different taper length at the current of 15 mA.

decreases with the increase of taper length. And the fitting slope efficiency first increases and then decreases, and finally becomes stable. The variation trends can be attributed to the influence of taper length on the lateral current and optical confinement of VCSEL and we will discuss in the later part of the article.

Fig. 4 shows the calculated P-I curves of LP_{01} and LP_{11} optical modes for the VCSELs with different taper length. Two transverse modes can be observed for all devices. However, it is interesting that, by increasing taper length, VCSEL will realize the transition from first order mode (LP_{11}) lasing to dual-mode lasing (LP_{01} and LP_{11}) and then to fundamental mode lasing (LP_{01}). This suggests that we can control the lasing mode of GaN VCSELs by adjusting the taper length.

To further analyze the underlying mechanism of varying threshold current, slope efficiency as well as lasing mode, we studied the lateral current and optical mode distribution of VCSELs with different taper length. Fig. 5(a) shows the spatial distributions of the current density within the QW. As shown in Fig. 5(a), flat aperture VCSEL will cause current crowding, and

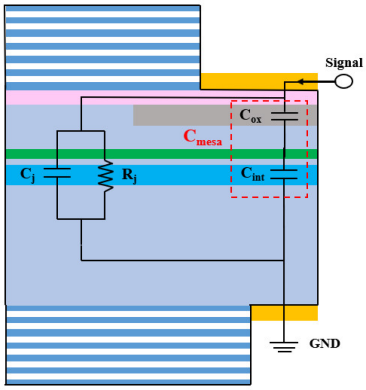

Fig. 8. Cross-sectional schematic of VCSEL with SiO_2-buried structure superimposed with its parasitics.

the current density is maximized near the edge of the current injection aperture. In comparison, for tapered aperture VCSEL, the current density gradually concentrates towards the center of the current injection aperture as the taper length increases. This suggests that a more uniform gain can be achieved by using tapered SiO_2-buried structure.

Fig. 5(b) shows the distribution of LP_{01} and LP_{11} optical modes within the QW of the devices with different taper length. Both LP_{01} and LP_{11} optical modes are distributed inside the current injection aperture. It is evident that the lower threshold current and higher slope efficiency can be achieved in the tapered aperture VCSEL, which is a direct result of the enhanced overlap between the current injection and the mode profile. In addition, the relative intensity of the LP_{01} and LP_{11} modes depends on the degree of overlap between the current injection and the mode profile as well. For example, when the taper length is larger than 1 μm, the current is more tightly confined to the peak region of LP_{01} mode, LP_{11} mode disappears, and single fundamental mode lasing is finally achieved. However, the full width at half maximum (FWHM) of LP_{01} and LP_{11} mode distributions in the lateral direction are widened with the increase of taper length, as shown in Fig. 5(b). As the taper length is increased, the volume of low index SiO_2 in the vicinity of the VCSEL center decreases. This results in a reduction in the effective index contrast inside and outside the current injection aperture. The optical confinement becomes worse when the taper length becomes longer. That is the reason why the slope efficiency decreases for tapered aperture VCSEL when increasing taper length, as shown in Fig. 3(b).

To better understand the observed redistribution of current inside the current injection aperture, we show the lateral potential profiles in Fig. 6(a). The potential profiles are strongly associated with the bias that is supported by the buried SiO_2 layer. Thus, the tapered SiO_2-buried structure can cause changes in potential, and a lateral energy barrier is generated. The lateral energy barrier is very useful to confine holes in the aperture and on the other, the barrier can prevent the holes from flowing into the region below the SiO_2 layer. In addition, the height of energy barrier increases as the taper length increases which is beneficial to more effectively confine carriers in the aperture. Fig. 6(b)

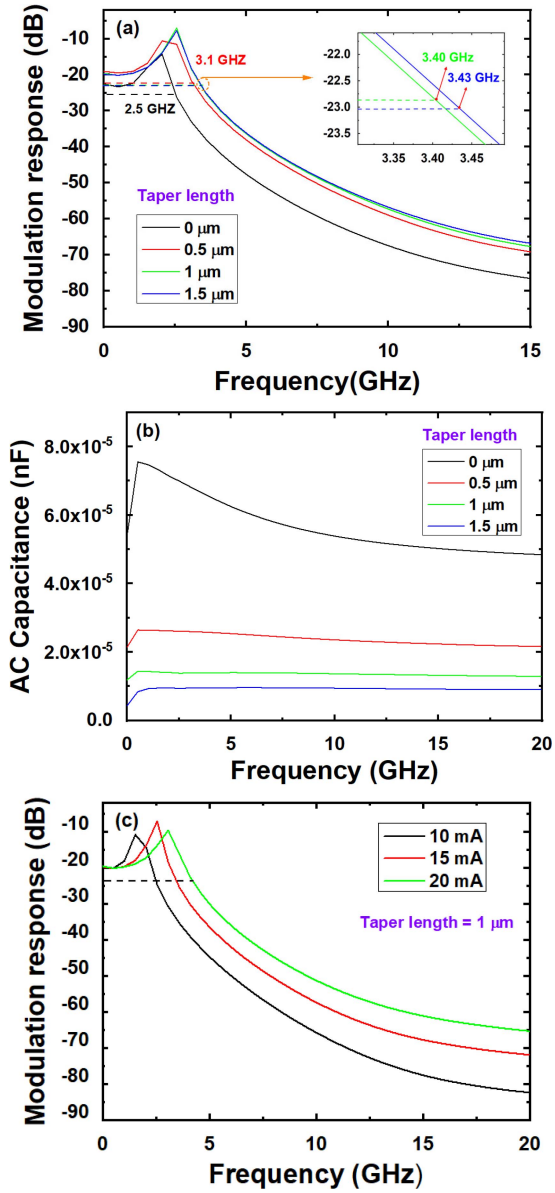

Fig. 9. (a) Calculated small-signal modulation response and (b) mesa capacitance for VCSELs with different taper length at the current of 15 mA. Inset shows the zoom-in 3dB frequency for VCSELs with 1 and 1.5 μm taper length. (c) Calculated small-signal modulation response as a function of injection current for the device with 1 μm taper length.

shows the lateral hole concentration profiles in p-GaN below the SiO_2 layer. Agreeing well with our conjecture, the larger energy barrier can cause hole accumulation in center region when the taper length becomes longer. Therefore, the lateral current confinement can be enhanced if the tapered structure is properly designed.

Fig. 7 shows calculated far-field distributions of VCSELs with different taper length. Far-fields are obtained from a superposition of LP_{01} and LP_{11} mode intensities. For flat aperture VCSEL (taper length is 0 μm), two side peaks appear, which means high-order transverse mode (LP_{11} mode) dominates. When the taper length is 0.5 μm, the far-field profile exhibits one broaden central peak, and the device shows multi transverse mode (LP_{01}

and LP_{11} mode) operation. Further increase of taper length to 1 μm, the far-field pattern profile is nearly perfect single-mode Gaussian shape with full-width at half-maximum shrinking to 2.4 degree. The VCSEL emits at fundamental mode (LP_{01} mode).

Since the bandwidth of VCSEL is affected by the extrinsic parasitics [22], the modulation bandwidth of tapered aperture VCSELs were also investigated. Fig. 8 shows the cross-sectional schematic of a VCSEL with SiO_2-buried structure superimposed with its parasitic elements. The circuit model, shown in Fig. 7, includes four elements: C_{ox}, C_{int}, C_j, and R_j. The mesa capacitance C_{mesa} is the oxide capacitance C_{ox} in series with the capacitance associated with the intrinsic region below the aperture C_{int}. The capacitance C_j represents the diode junction capacitance in the apertured area where current flows. R_j denotes the diode junction resistance for the active region.

The calculated frequency response characteristics for VCSELs with different taper length are presented in Fig. 9(a). We can find that, as the taper length increases from 0 μm to 1.5 μm, the 3dB frequencies for VCSELs are increased from 2.5 GHz to 3.43 GHz at the current of 15 mA. Fig. 9(b) shows the simulated mesa capacitance of VCSELs with different taper length. The larger taper length will reduce the C_{ox}, and thus the smaller C_{mesa}. Therefore, the larger taper length can increase the modulation bandwidth. In addition, as the injection current increases, the 3dB frequencies for device also increases, as shown in Fig. 9(c). We believe that the tapered structure can be properly designed in the way of achieving single fundamental mode lasing while maintaining a large 3dB frequency.

IV. Conclusion

In conclusion, we theoretically investigated the performance of GaN-based VCSELs with tapered SiO_2-buried structure by numerical simulations. By introducing tapered aperture structure, the current crowding problem of VCSEL is mitigated, and can provide the lower threshold current and higher slope efficiency. In addition, by increasing taper length, single fundamental mode operation and larger 3dB frequency can be achieved. This work provides a deeper understanding on GaN-based VCSEL with tapered SiO_2 buried structure. Such a structure is compatible with existing GaN VCSEL manufacturing processes and can have important significance for the development of high performance GaN-based VCSELs.

References

[1] A. Liu, P. Wolf, J. A. Lott, and D. Bimberg, "Vertical-cavity surface-emitting lasers for data communication and sensing," *Photon. Res.*, vol. 7, no. 2, pp. 121–136, Feb. 2019, doi: 10.1364/PRJ.7.000121.

[2] K. Iga, "VCSEL: Born small and grown big," *Vertical External Cavity Surf. Emitting Lasers*, vol. 11263, Mar. 2020, Art. no. 1126302, doi: 10.1117/12.2554953.

[3] S. C. Tian, M. Ahamed, and D. Bimberg, "Progress in short wavelength energy-efficient high-speed vertical-cavity surface-emitting lasers for data communication," *Photonics*, vol. 10, no. 4, pp. 1–17, Apr. 2023, doi: 10.3390/photonics10040410.

[4] H. T. Cheng, Y. C. Yang, T. H. Liu, and C. H. Wu, "Recent advances in 850 nm VCSELs for high-speed interconnects," *Photonics*, vol. 9, no. 2, pp. 1–27, Feb. 2022, doi: 10.3390/photonics9020107.

[5] T. C. Yu, W. T. Huang, W. B. Lee, C. W. Chow, S. W. Chang, and H. C. Kuo, "Visible light communication system technology review: Devices, architectures, and applications," *Crystals*, vol. 11, no. 9, Sep. 2021, Art. no. 1098, doi: 10.3390/cryst11091098.

[6] S. Shen et al., "GHz modulation bandwidth from single-longitudinal mode violet-blue VCSEL using nonpolar InGaN/GaN QWs," in *Proc. IEEE Conf. Lasers Electro-Opt.*, 2016, pp. 1–2, doi: 10.1364/CLEO_SI.2016.STh1L.2.

[7] E. Hashemi et al., "Analysis of structurally sensitive loss in GaN-based VCSEL cavities and its effect on modal discrimination," *Opt. Exp.*, vol. 22, no. 1, pp. 411–426, Jan. 2014, doi: 10.1364/OE.22.000411.

[8] S. Hang et al., "On the origin for the hole confinement into apertures for GaN-based VCSELs with buried dielectric insulators," *Opt. Exp.*, vol. 28, no. 6, Mar. 2020, Art. no. 8668, doi: 10.1364/OE.385787.

[9] J. T. Leonard et al., "Nonpolar III-nitride vertical-cavity surface-emitting lasers incorporating an ion implanted aperture," *Appl. Phys. Lett.*, vol. 107, no. 1, Jul. 2015, Art. no. 011102, doi: 10.1063/1.4926365.

[10] S. M. Mishkat-Ul-Masabih, A. A. Aragon, M. Monavarian, T. S. Luk, and D. F. Feezell, "Electrically injected nonpolar GaN-based VCSELs with lattice-matched nanoporous distributed Bragg reflector mirrors," *Appl. Phys. Exp.*, vol. 12, no. 3, Mar. 2019, Art. no. 036504, doi: 10.7567/1882-0786/ab0576.

[11] J. T. Leonard et al., "Nonpolar III-nitride vertical-cavity surface-emitting laser with a photoelectrochemically etched air-gap aperture," *Appl. Phys. Lett.*, vol. 108, no. 3, Jan. 2016, Art. no. 031111, doi: 10.1063/1.4940380.

[12] R. Iida et al., "GaN-based vertical cavity surface emitting lasers with lateral optical confinements and conducting distributed Bragg reflectors," *Jpn. J. Appl. Phys.*, vol. 59, no. SG, Feb. 2020, Art. no. SGGE08, doi: 10.35848/1347-4065/ab6e05.

[13] M. Kuramoto et al., "Enhancement of slope efficiency and output power in GaN-based vertical-cavity surface-emitting lasers with a SiO_2-buried lateral index guide," *Appl. Phys. Lett.*, vol. 112, no. 11, Mar. 2018, Art. no. 111104, doi: 10.1063/1.5020229.

[14] R. Xu et al., "Effects of lateral optical confinement in GaN VCSELs with double dielectric DBRs," *IEEE Photon. J.*, vol. 12, no. 2, Apr. 2020, Art. no. 1501708, doi: 10.1109/JPHOT.2020.2979564.

[15] T. Hamaguchi et al., "Lateral optical confinement of GaN-based VCSEL using an atomically smooth monolithic curved mirror," *Sci. Rep.*, vol. 8, no. 1, Jul. 2018, Art. no. 10350, doi: 10.1038/s41598-018-28418-6.

[16] G. Cosendey, A. Castiglia, G. Rossbach, J. F. Carlin, and N. Grandjean, "Blue monolithic AlInN-based vertical cavity surface emitting laser diode on free-standing GaN substrate," *Appl. Phys. Lett.*, vol. 101, no. 15, Oct. 2012, Art. no. 151113, doi: 10.1063/1.4757873.

[17] M. Kuramoto, S. Kobayashi, T. Akagi, K. Tazawa, H. Tanaka, and T. Takeuchi, "Nano-height cylindrical waveguide in GaN-based vertical-cavity surface-emitting lasers," *Appl. Phys. Exp.*, vol. 13, no. 8, Aug. 2020, Art. no. 082005, doi: 10.35848/1882-0786/aba45b.

[18] N. Hayashi et al., "A GaN-based VCSEL with a convex structure for optical guiding," *Physica Status Solidi*, vol. 215, no. 10, May 2018, Art. no. 1700648, doi: 10.1002/pssa.201700648.

[19] R. Michalzik Ed., *VCSELs: Fundamentals, Technology and Applications of Vertical-Cavity Surface-Emitting Lasers*, vol. 166. Berlin, Germany: Springer, 2013, pp. 127–138, doi: 10.1007/978-3-642-24986-0.

[20] W. J. Liu, X. L. Hu, L. Y. Ying, J. Y. Zhang, and B. P. Zhang, "Room temperature continuous wave lasing of electrically injected GaN-based vertical cavity surface emitting lasers," *Appl. Phys. Lett.*, vol. 104, no. 25, Jun. 2014, Art. no. 251116, doi: 10.1063/1.4885384.

[21] Y. Wang, T. Yang, L. Shi, Y. Chen, Y. Mei, and B. P. Zhang, "Simulation of performance enhancement of GaN-based VCSELs by composition gradient InGaN last-quantum barrier," *Semicond. Sci. Technol.*, vol. 38, no. 12, Dec. 2023, Art. no. 125003, doi: 10.1088/1361-6641/ad03fd.

[22] M. Feng, C.-H. Wu, and N. Holonyak, "Oxide-confined VCSELs for high-speed optical interconnects," *IEEE J. Quantum Electron.*, vol. 54, no. 3, Jun. 2018, Art. no. 2400115, doi: 10.1109/JQE.2018.2817068.